Rescattering photoelectron spectroscopy of the CO_2 molecule: Towards experimental discrimination between theoretical target structure models

Misaki Okunishi,[1] Yuta Ito,[1] Vandana Sharma,[2] Shejuty Aktar,[1]
Kiyoshi Ueda,[1] Robert R. Lucchese,[3] Andrey I. Dnestryan,[4,5]
Oleg I. Tolstikhin,[4] Shunsuke Inoue,[6] Hirokazu Matsui,[6] and Toru Morishita[7,6]

[1]*Institute of Multidisciplinary Research for Advanced Materials, Tohoku University, 2-1-1 Katahira, Aoba-ku, Sendai-shi 980-8577, Japan*

[2]*Department of Physics, Indian Institute of Technology-Hyderabad, Kandi, Sangareddy, Telangana 502285 India*

[3]*Lawrence Berkeley National Laboratory, Berkeley California, 94720-8196, United States*

[4]*Moscow Institute of Physics and Technology, Dolgoprudny 141700, Russia*

[5]*National Research University Higher School of Economics, Moscow 101000, Russia*

[6]*Department of Engineering Science, The University of Electro-Communications 1-5-1 Chofu-ga-oka, Chofu-shi, Tokyo 182-8585, Japan*

[7]*Institute for Advanced Science, The University of Electro-Communications, 1-5-1 Chofu-ga-oka, Chofu-shi, Tokyo 182-8585, Japan*

(Dated: August 15, 2019)

Abstract

Photoelectron momentum distributions (PEMDs) generated in strong-field ionization of randomly oriented CO_2 molecules by intense infrared laser pulses at 1300, 1450, and 1650 nm wavelengths are measured experimentally and analyzed theoretically. The experimental PEMDs extracted along the outermost backward rescattering caustic are well reproduced by theoretical calculations based on the recently derived factorization formula with an analytical returning photoelectron wave packet (RWP). The sensitivity of the theoretical results to the target structure models used in the calculations is investigated. It is shown that RWPs obtained in the single-active-electron (SAE) approximation and by the Hartree-Fock method have only minor differences. On the other hand, differential cross sections (DCSs) for elastic scattering of a photoelectron on the parent molecular ion calculated by *ab initio*, SAE, and independent-atom model methods are considerably different. This difference almost disappears after averaging over molecular orientations, so the present experiment does not enable us to discriminate between the different target structure models. However, we show that such a discrimination should become possible by measuring PEMD with aligned molecules. This will provide an access to the rich target structure information contained in the DCS.

I. INTRODUCTION

In the past decade laser-induced electron diffraction (LIED) from gas-phase molecules, which utilizes the elastically rescattered photoelectrons generated by intense laser pulses, was successfully applied to extracting molecular geometry [1–5]. The LIED was originally proposed theoretically as a technique for ultrafast dynamic imaging of molecules using intense laser pulses [6] and then its potential was demonstrated experimentally [7]. A powerful method for extracting molecular structure information from photoelectron momentum distributions (PEMDs) generated by strong-field ionization of target molecules was proposed in Ref. [8]. It was suggested that strong-field PEMDs in the region dominated by nearly backward rescattered photoelectrons factorize into the differential cross sections (DCS) for elastic scattering of a photoelectron on the parent ion and a returning photoelectron wave packet (RWP). The factorization formula was inferred from numerical calculations, so that no explicit expression for the RWP could be given. It was assumed to hold near the outer high-energy boundary of the PEMD, along a circle in the photoelectron momentum space corresponding to rescattering with the largest incident momentum for a given pulse shape. The RWP was assumed to be independent of the position along the circle, so the experimental PEMD extracted along the circle up to a constant factor coincides with the DCS. This approach was verified experimentally for rare gas atoms [9, 10] and several simple molecules [11, 12]. Later, it was extended in an *ad hoc* way by applying the extraction procedure in the inner region of the PEMD [1], at smaller rescattering momenta than were initially considered [8], to improve statistics of photoelectron counts.

Recently, the factorization formula underlying the approach initiated in Ref. [8] was derived [13] within the adiabatic theory [14]. It was shown that the formula holds in the vicinity of the outermost backward rescattering caustic. Only near the backward rescattering direction can the caustic be approximated by the circle considered in Ref. [8]. Furthermore, an analytical expression for the RWP was obtained. The theory developed in Ref. [13] has elevated the approach of Ref. [8] to a quantitative level, which has been confirmed by comparing results predicted by the analytical formula with PEMDs obtained by solving the time-dependent Schrödinger equation for a number of atomic potentials. The performance of the theory was demonstrated by extracting DCSs from experimental PEMDs for the Xe atom [15] in which the most weakly bound electrons are in a fully occupied p shell of the

target, the diatomic CO which has a fully occupied σ highest occupied molecular orbital (HOMO), and NO which has a singly occupied π HOMO [16]. In the present study, we extend the application of the theory to rescattering photoelectron spectroscopy of a triatomic CO_2 molecule which has a fully occupied HOMO of π symmetry. The main goal of this study is to investigate the sensitivity of the molecular imaging procedure to the target structure information used in implementing the factorization formula and thus to pave the way towards experimental discrimination between theoretical target structure models.

The paper is organized as follows. In Sec. II, we briefly outline the experimental setup used to measure the PEMDs for CO_2 molecules generated by intense near-infrared laser pulses at 1300, 1450, and 1650 nm wavelengths. In Sec. III, we describe our theoretical procedure based on the factorization formula derived in Ref. [13] and introduce several target structure models used to implement this formula in the present study. In Sec. IV, we analyze the dependence of the RWPs and DCSs obtained by the different methods on the alignment angle between the molecular axis and the ionizing field and the photoelectron scattering angle. Finally, we compare the experimental and theoretical PEMDs along the outermost caustic for the three laser wavelengths considered. Section V concludes the paper.

II. EXPERIMENT

The present experimental setup is similar to the one used in previous studies [4, 5, 16]. The output of a Ti:Sapphire laser system (800 nm, 100 fs, 1.5 mJ/pulse, 1 kHz) was injected into an optical parametric amplifier to convert the wavelength to 1300, 1450, and 1650 nm. The resulting linearly polarized laser beam was introduced into a high vacuum chamber through a half waveplate and focused on CO_2 molecules by an $f = 75$ mm concave mirror. The CO_2 gas was effusively expanded into the chamber. A typical working pressure was about $1 - 2 \times 10^{-4}$ Pa and the base pressure was less than 1×10^{-8} Pa. We used a 264 mm long field-free time-of-flight (TOF) spectrometer to measure photoelectron momentum. Photoelectrons released from the molecules were detected by a multi-channel plate with a limited solid angle ($\approx 0.0014 \times 4\pi$ sr) through the drift tube of the TOF spectrometer. The waveplate was rotated with a constant angular velocity of one rotation per minute to obtain the flight time of photoelectrons as a function of angles between the laser polarization axis and the direction of electron emission. The measured angle-resolved TOFs were transformed

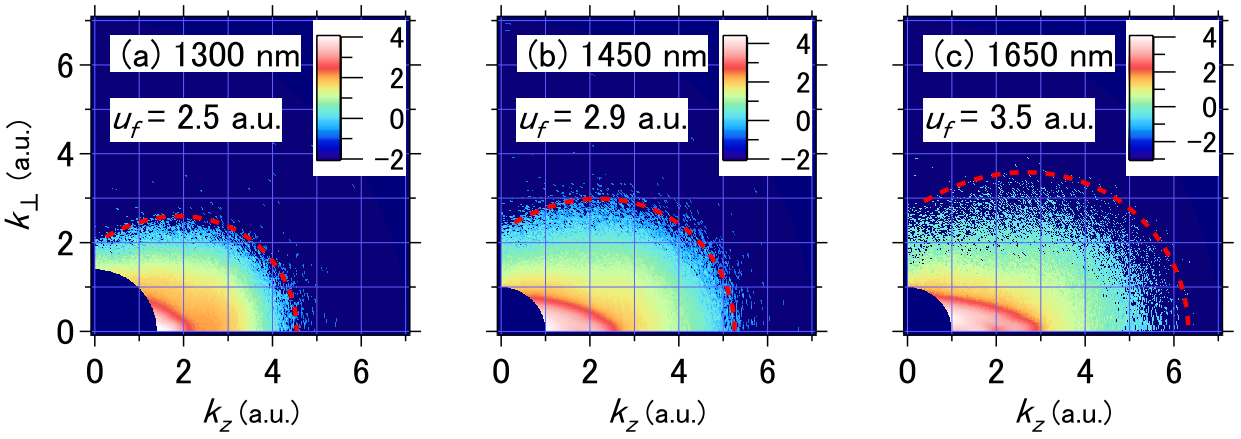

FIG. 1. Experimental PEMDs for CO_2 measured with infrared laser pulses at (a) 1300 nm, (b) 1450 nm and (c) 1650 nm displayed on a logarithmic scale (arbitrary units) with false colors. The PEMDs are axially symmetric about the k_z axis and mirror-symmetric with respect to the (k_x, k_y) plane. The dashed (red) lines show the outermost quantum caustic $\tilde{\mathbf{k}}(\theta)$ determined by effective peak field amplitudes (a) $\bar{F}_0 = 0.070$ a.u., (b) $\bar{F}_0 = 0.072$ a.u., and (c) $\bar{F}_0 = 0.077$ a.u. in the interval of scattering angles $60° \leqslant \theta \leqslant 180°$. The values of u_f indicate the corresponding incident momenta of rescattering at the caustic for $\theta = 180°$.

into the density of events in three-dimensional photoelectron momentum space, which up to a constant normalization factor coincides with the PEMD. The PEMD for randomly oriented molecules is axially symmetric about the polarization axis and mirror-symmetric under the inversion of its direction. Results obtained for the three wavelengths considered are shown in Fig. 1.

III. THEORY

The theoretical modeling of the results follows a procedure introduced in Ref. [16]. It is based on the analytical factorization formula describing the PEMD near a backward rescattering caustic recently derived [13] within the adiabatic theory [14]. Here we briefly summarize the procedure and then discuss its implementation for the present molecule.

A. Factorization formula

The laser field is assumed to be polarized along the z axis of the laboratory frame and given by $\mathbf{F}(t) = F(t)\mathbf{e}_z$ with $F(t) = F_0 \exp[-(2t/T)^2]\cos\omega t$, where F_0 is the peak field amplitude, ω is the laser frequency, and $\sqrt{\ln 2}\,T$ is the full width at half maximum of the pulse. We first discuss the PEMD resulting from ionization of a space-fixed molecule. The orientation of the molecule is described by the Euler angles $(\alpha, \beta, \gamma = 0)$ defining a rotation from the laboratory frame to the molecular frame [17]. Here β is the angle between the polarization axis and the molecular axis and α describes the rotation of the molecular axis about the polarization axis. We consider ionization from the HOMO in CO_2. In the general case, there exist several direct and rescattering trajectories contributing to the PEMD at a given photoelectron momentum $\mathbf{k} = (k_x, k_y, k_z)$ [14]. However, near the outer boundary of the distribution, only contributions from one pair of long and short nearly backward rescattered trajectories [18] originating from the main maximum of $|F(t)|$ survive. In the adiabatic regime, the incident momentum of an electron arriving for rescattering is parallel to the polarization axis [14]. The two trajectories coalesce at a caustic in the photoelectron momentum space which is a surface of revolution about the k_z axis. This caustic is a classical object, its shape is completely determined by the field $F(t)$. We parameterize it by spherical scattering angles $\Omega = (\theta, \varphi)$ characterizing the rescattering event for the coalesced trajectories measured relative to the direction of the incident momentum. The experimental PEMDs are considered in a half-plane with coordinates $(k_\perp, k_z)$, where $k_\perp = \sqrt{k_x^2 + k_y^2}$ (see Fig. 1). The caustic crosses this half-plane along a line $\mathbf{k}(\theta) = (k_\perp(\theta), k_z(\theta))$ defined in Ref. [13]. The two saddle points describing the contributions of the coalescing trajectories to the PEMD coalesce at the corresponding quantum caustic which is also a surface of revolution about the k_z axis obtained from the classical caustic by a shift in the direction of the external normal to it. The quantum caustic crosses the half-plane $(k_\perp, k_z)$ along a line $\tilde{\mathbf{k}}(\theta) = (\tilde{k}_\perp(\theta), \tilde{k}_z(\theta))$ defined in Ref. [13] (see dashed red lines in Fig. 1). The shift from $\mathbf{k}(\theta)$ to $\tilde{\mathbf{k}}(\theta)$ depends on the energy $E_\beta(t)$ of the Siegert state emerging from the unperturbed HOMO in the presence of a static electric field equal to the instantaneous laser field $F(t)$ at the moment of ionization [19, 20]. The Siegert energy is complex, its real part accounts for the Stark shift of the HOMO and its imaginary part defines the instantaneous tunneling ionization rate $\Gamma_\beta(t) = -2\,\mathrm{Im}\,E_\beta(t)$. The factorization formula for the PEMD holds in the

vicinity of the quantum caustic. In particular, at the caustic the PEMD is given by [13]

$$P(\Omega;\alpha,\beta) = |f_\beta(u_f(\theta),\Omega_\alpha)|^2\, W_\beta(\theta). \tag{1}$$

Here $f_\beta(k,\Omega)$ is the scattering amplitude defining the DCS $d\sigma_\beta/d\Omega = |f_\beta(k,\Omega)|^2$ for elastic scattering of an electron with incident momentum $k\mathbf{e}_z$ by the molecular ion with the orientation angles $\alpha = 0$ and β, $u_f(\theta)$ is the incident momentum of rescattering at the classical caustic $\mathbf{k}(\theta)$, and the notation $\Omega_\alpha = (\theta, \varphi - \alpha)$ indicates that the DCS depends only on the difference between the angles φ and α. The second factor in Eq. (1) is the RWP taken at the quantum caustic $\tilde{\mathbf{k}}(\theta)$ given by

$$W_\beta(\theta) = |\mathrm{Ai}(0)|^2 \left|\frac{2}{S_r'''(\theta)}\right|^{2/3} \frac{4\pi^2 |A_\beta(t_i(\theta))|^2}{(t_r(\theta)-t_i(\theta))^3 |F(t_i(\theta))|} \exp\left[-\int_{-\infty}^{t_i(\theta)} \Gamma_\beta(t)dt\right], \tag{2}$$

where $\mathrm{Ai}(0) \approx 0.355$ is the Airy function at zero argument. Here $t_i(\theta)$ and $t_r(\theta)$ are the moments of ionization and rescattering, respectively, and $S_r'''(\theta)$ is a derivative of the corresponding classical action. These quantities, as well as $u_f(\theta)$, are kinematic characteristics of the rescattering event at the classical caustic $\mathbf{k}(\theta)$; explicit formulas defining them are given in Ref. [13]. In addition, Eq. (2) contains properties of the Siegert state in the instantaneous laser field $F(t)$, namely, the transverse momentum distribution (TMD) amplitude taken at zero transverse momentum $A_\beta(t)$ [19, 21] and the ionization rate $\Gamma_\beta(t)$.

To obtain theoretical results for randomly oriented molecules, we have to average Eq. (1) over the molecular orientation angles α and β. The RWP (2) does not depend on φ and α, so the PEMD (1) depends only on the difference between these angles through the DCS. Then the integration over α amounts to that over φ, and we obtain

$$S(\theta) = \frac{1}{4\pi}\int_0^{2\pi}\int_0^{\pi} P(\Omega;\alpha,\beta)\sin\beta d\beta d\alpha \tag{3a}$$

$$= \frac{1}{2}\int_0^{\pi} \sigma_\beta(\theta) W_\beta(\theta)\sin\beta d\beta, \tag{3b}$$

where

$$\sigma_\beta(\theta) = \int_0^{2\pi} |f_\beta(u_f(\theta),\Omega)|^2 \frac{d\varphi}{2\pi} \tag{4}$$

is the DCS averaged over the azimuthal scattering angle φ. The thus calculated function $S(\theta)$ is to be compared with experimental PEMDs extracted along the quantum caustic $\tilde{\mathbf{k}}(\theta)$. This procedure has been demonstrated by comparing theoretical and experimental results for NO and CO molecules [16]. Below we apply it to the analysis of the present experimental results for the CO_2 molecule.

B. Target structure information

To implement the factorization formula (1) some target structure information is needed. This includes the amplitude $f_\beta(k,\Omega)$ for elastic scattering of an electron on the parent molecular ion defining the DCS factor and the energy $E_\beta(t)$, ionization rate $\Gamma_\beta(t)$, and the TMD amplitude $A_\beta(t)$ characterizing the Siegert state and defining the shift between the classical $\mathbf{k}(\theta)$ and quantum $\tilde{\mathbf{k}}(\theta)$ caustics and the RWP factor. Neither of these quantities can be calculated exactly for many-electron molecules, so one has to resort to the use of suitable approximations. Here we discuss such approximations applicable to general molecules. Since we wish to investigate the sensitivity of the theoretical results to the different approximations, we consider several methods of calculating each of the target properties needed.

We begin with the properties of the Siegert state. They are described using the leading-order approximation of the weak-field asymptotic theory (WFAT) [22]. In this approximation, the Siegert energy is given by the first-order perturbation theory. Since there is no linear Stark shift for the present nonpolar molecule, the Siegert energy $E_\beta(t)$ is approximated by the energy E_0 of the unperturbed HOMO. In the same approximation, the ionization rate and the TMD amplitude are given by [22, 23]

$$\Gamma_\beta(t) = \left[|G_{00}(\beta)|^2 + \frac{F}{2\varkappa^2}|G_{01}(\beta)|^2\right] W_{00}(F) \tag{5}$$

and

$$|A_\beta(t)|^2 = \frac{4\pi\varkappa}{F}|G_{00}(\beta)|^2 W_{00}(F), \tag{6}$$

where $F = |F(t)|$, $\varkappa = \sqrt{-2E_0}$, $G_{00}(\beta)$ and $G_{01}(\beta)$ are structure factors for the dominant and next-to-the-dominant ionization channels, respectively, and

$$W_{00}(F) = \frac{\varkappa}{2}\left(\frac{4\varkappa^2}{F}\right)^{2/\varkappa-1} \exp\left(-\frac{2\varkappa^3}{3F}\right) \tag{7}$$

is the field factor. The structure factors are properties of the unperturbed HOMO. We calculate them using two different approaches. In the first approach the HOMO is obtained by the Hartree-Fock (HF) method. We use an integral representation for structure factors developed in Ref. [24] recently implemented for arbitrary polyatomic molecules [25] on the basis of the quantum chemistry package GAMESS [26]. In the HF calculation on CO_2, the orbital energy of the HOMO is $E_0 = -0.544\,905$ a.u. This approach is referred to below as WFAT-HF. The second approach is similar to the one used in Ref. [16]. In this approach,

the HOMO is obtained in the single-active-electron (SAE) approximation by solving the time-independent Schrödinger equation with a molecular potential modeled by the sum of three individual atomic potentials,

$$V(\mathbf{r}) = -\sum_{i=1}^{3} \frac{Z_i(r_i)}{r_i}, \tag{8}$$

where $i = 1$, 2, and 3 refer to the O, C, and O atoms, respectively. Here $r_i = |\mathbf{r} - \mathbf{R}_i|$ are the distances from the active electron to the nuclei located at $\mathbf{R}_1 = -\mathbf{R}$, $\mathbf{R}_2 = \mathbf{0}$, and $\mathbf{R}_3 = +\mathbf{R}$, where $\mathbf{R} = (R\sin\beta, 0, R\cos\beta)$ and $R = 2.1961$ a.u. is the equilibrium distance between each of the O and the C nuclei in CO_2. We use coordinate-dependent effective charges $Z_i(r)$ defined by [27]

$$Z_i(r) = a_i - (b_i - 1)\{1 - [(v_i/u_i)(e^{u_i r} - 1) + 1]^{-1}\}. \tag{9}$$

Here $a_i = Z_i(0)$ is the nuclear charge for the corresponding atom in the molecule set equal to 6 or 8 for the C and O atoms, respectively. The other parameters are chosen in such a way that the ionization potential of the HOMO in the model is the same as the experimental ionization potential of 0.5663 a.u. [28]; note that this energy is slightly larger than the Koopmans' theorem ionization potential in the HF calculation. This is achieved with $b_1 = b_3 = 8.67$, $u_1 = u_3 = 2.4625$, and $v_1 = v_3 = 1.3615$, for the O atoms, and $b_2 = 6.66$, $u_2 = 2.1174$, and $v = 1.0485$, for the C atom. Having constructed the HOMO, the structure factors were calculated as described in Refs. [22, 23]. We refer to this approach as WFAT-SAE. We mention that within the SAE approach the properties of the Siegert state can be accurately calculated beyond the weak-field approximation using the method developed in Refs. [19–21]. Such calculations are feasible for diatomics, but become difficult for larger molecules. At the same time, *ab initio* many-electron calculations of tunneling ionization rates of molecules are so far limited to a few cases [29]. In this situation the WFAT [22] is indispensable for calculating the RWP (2).

We next discuss the DCS factor in Eq. (1). We use three approaches to calculate the DCS for electron-ion elastic scattering: (i) *ab initio* scattering calculations in the static-exchange approximation, (ii) SAE scattering calculations with the potential (8) implemented as described in Ref. [16], and (iii) independent-atom model (IAM) calculations in which the scattering amplitude for a molecule is approximated by the sum of scattering amplitudes for

each atom in the molecule, and the atomic scattering amplitudes are taken from a database [30, 31]. These approaches are referred to as *ab initio*, SAE, and IAM, respectively.

The *ab initio* calculations for the scattering of an electron from a molecular ion used the ePolyScat package [32, 33]. These employed a single-center expansion with $L_{\max} = 80$ and used the same geometry as was used in the SAE model. The target molecular orbitals were obtained from a HF calculation on the neutral target using an aug-cc-pVTZ Dunning correlation consistent one-electron basis set [34, 35].

We emphasize that all the methods to calculate the target structure information described above are general in the sense that their implementation can be extended to larger polyatomic molecules.

IV. RESULTS AND DISCUSSION

Figure 1 shows experimental PEMDs for CO_2 molecules ionized by laser pulses at the three wavelengths considered. In order to compare these results with the theoretical calculations, we need to determine the position of the quantum caustic $\tilde{\mathbf{k}}(\theta)$. To do this, we need to know the peak field amplitude F_0 of the pulse. It is found using a procedure introduced in Ref. [16]. We are interested in the outermost quantum caustic produced by ionization of molecules by the most intensive field, that is, in the central part of the focal volume, in space, and near the maximum of the pulse envelope, in time. Only near this caustic the PEMD is determined by contributions from only one pair of long and short rescattering trajectories and the factorization formula (1) holds; in the inner part of the distribution, several pairs of rescattering trajectories with *different* incident momenta contribute, so no common DCS can be factorized [13]. The outermost caustic goes along the outer boundary of the PEMD. To find it, we consider the PEMD near its boundary along the k_z axis and take a point where the measured signal is a few hundred times weaker than that at the onset of the plateau at smaller k_z. By fitting the position of this point to the theoretical value of $\tilde{\mathbf{k}}(\theta = 180^\circ)$, we find an effective peak field amplitude $\bar{F}_0$ of the pulse; the results are given in the caption to Fig. 1. The PEMD rapidly decays in the interval of k_z considered, so the uncertainty in the value of $\bar{F}_0$ is small. The knowledge of $\bar{F}_0$ determines the position of the caustic $\tilde{\mathbf{k}}(\theta)$ at all scattering angles θ (shown by dashed red lines in the figure), as well as all the kinematic characteristics needed to implement Eq. (1), such as the incident momentum

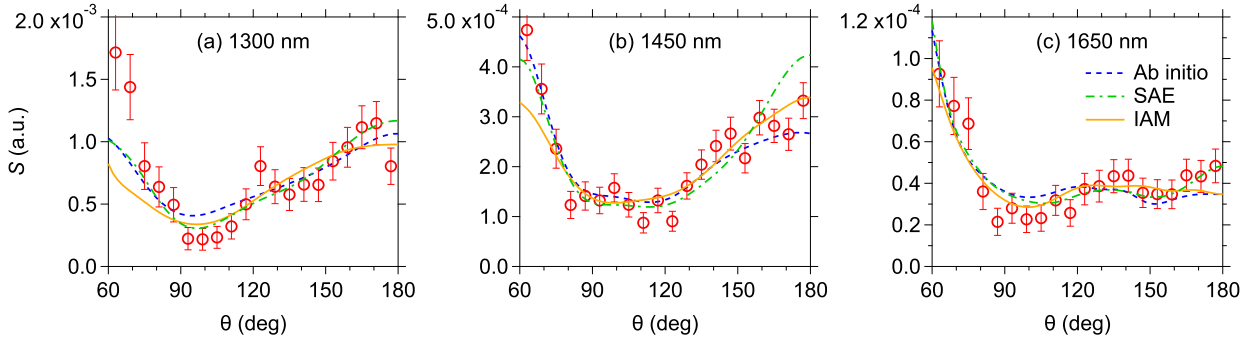

FIG. 2. Experimental (red circles) and theoretical (lines) PEMDs as functions of the scattering angle θ along the outermost quantum caustic $\tilde{\mathbf{k}}(\theta)$ for CO_2 ionized by infrared laser pulses at (a) 1300 nm, (b) 1450 nm, and (c) 1650 nm. The experimental PEMDs are extracted along the dashed red lines in Fig. 1. The theoretical PEMDs are obtained from Eq. (3b) using the DCSs calculated by *ab initio* (dashed blue lines), SAE (dash-dotted green lines), and IAM (solid orange lines) methods. Absolute values of the PEMDs are obtained by the SAE method. The other theoretical and experimental results are normalized to fit the SAE results in the interval $70° \leqslant \theta \leqslant 170°$.

of rescattering $u_f(\theta)$ (the values of $u_f = u_f(\theta = 180°)$ are indicated in the figure). The experimental results, using momenta extracted along the caustic, are shown by red circles in Fig. 2, where they are compared to the theoretical results.

The theoretical PEMDs are calculated using Eqs. (1)-(4). We first discuss results obtained by the different methods for each of the two factors in the integrand in Eq. (3b) as functions of the scattering angle θ and the molecular alignment angle β, and then perform the integration over β and compare with the experimental results shown in Fig. 2.

We have calculated the RWP (2) for each of the three laser pulses considered in the experiment using the WFAT-HF and WFAT-SAE approaches. The WFAT-HF results are shown in Fig. 3. It turns out that the shape of the dependence of the WFAT-SAE results on θ and β is similar to that shown in Fig. 3. The results of the two approaches differ almost only by a common factor. This difference originates from the different values of the energy E_0 of the HF and SAE HOMOs which strongly affects the overall magnitude of the RWP via the field factor (7) defining the ionization rate (5) and the TMD amplitude (6). The structure factors calculated by the two approaches are very close to each other. The experimental PEMDs are known up to a common factor. This means that the present experimental results do not enable us to discriminate between the WFAT-HF and WFAT-

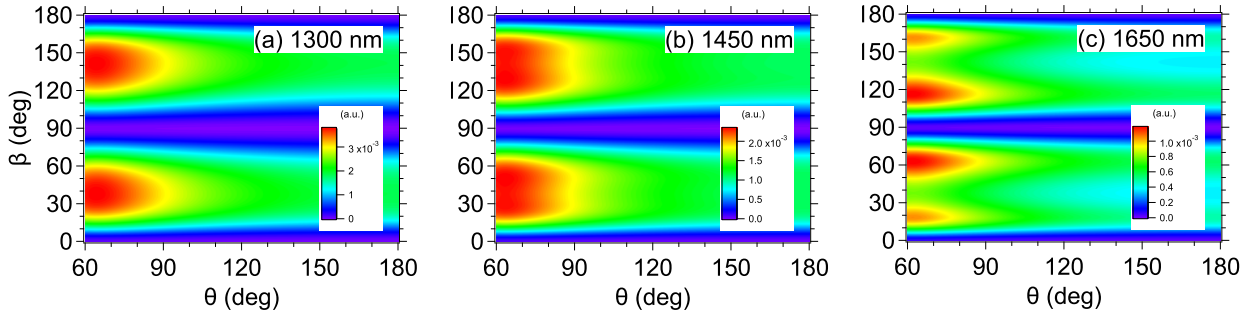

FIG. 3. RWPs defined by Eq. (2) as functions of the scattering angle θ and the molecular alignment angle β calculated using the WFAT-HF approach for the three laser pulses considered.

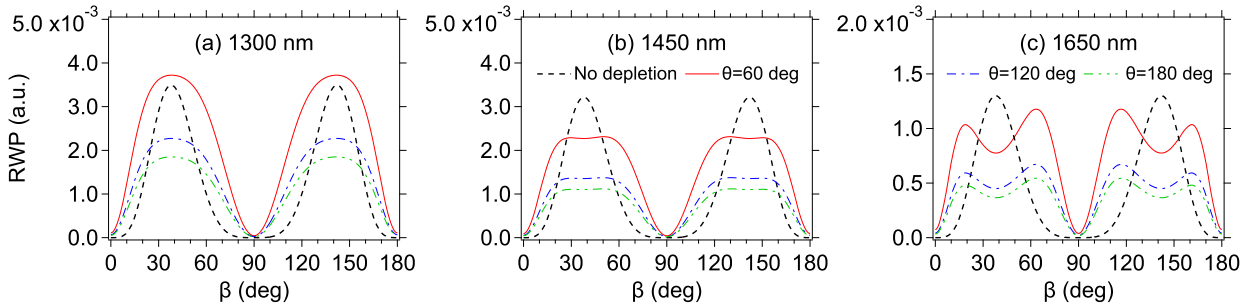

FIG. 4. Cuts of the RWPs shown in Fig. 3 as functions of the molecular alignment angle β at $\theta = 60°$ (solid red lines), 120° (dash-dotted blue lines), and 180° (dash-double-dotted green lines). The dashed black lines show the cuts at $\theta = 60°$ calculated without the depletion factor in Eq. (2). These results are multiplied by a factor bringing them to the scale of the figure.

SAE approaches to calculating the RWP. Accordingly, to simplify the discussion, we ignore the difference between these approaches in the following.

The RWPs shown in Fig. 3 demonstrate rather strong dependence on the alignment angle β. To illustrate this dependence in more detail, we show in Fig. 4 cuts of the RWPs as functions of β at three values of θ. The dependence on β is described by two factors in Eq. (2): the TMD amplitude and the last exponential factor accounting for depletion of the ionizing orbital. To disentangle the effects of these factors, we also show cuts of RWPs calculated with the depletion factor in Eq. (2) omitted. The latter cuts depend on β only through the structure factor in Eq. (6). This factor defines the orientation dependence of the ionization rate (5) in the weak-field limit [22, 23]. It has two peaks located near $\beta = 40°$ and 140° which reflect the two-lobe shape of the HOMO in CO_2. For the 1300 nm laser pulse depletion effects are rather weak, so cuts of the RWP shown in Fig. 4(a) calculated with

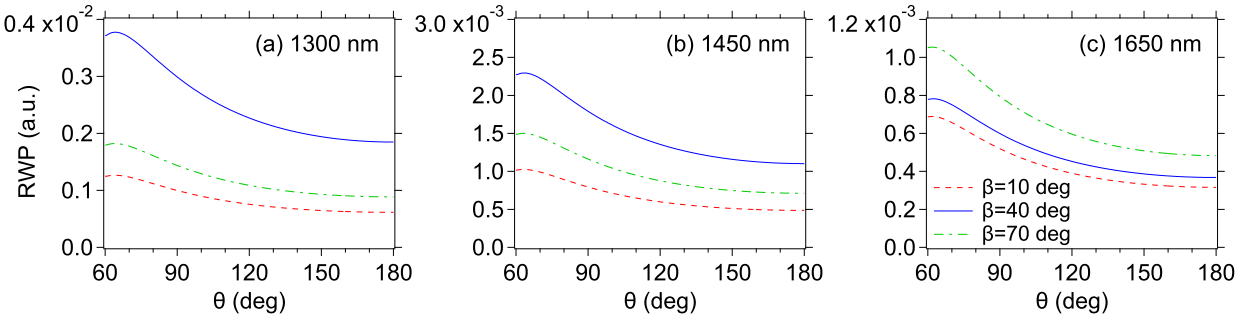

FIG. 5. Cuts of the RWPs shown in Fig. 3 as functions of the scattering angle θ at $\beta = 10°$ (dashed red lines), 40° (solid blue lines), and 70° (dash-dotted green lines).

and without the depletion factor have qualitatively similar two-peak shapes. However, as the laser wavelength grows, depletion begins to play a more important role, which modifies the shape of the RWP. Thus, flat plateaus are formed at the top of the peaks in the cuts of the RWP with depletion for the 1450 nm pulse shown in Fig. 4(b) which turn into dips in the cuts for the 1650 nm pulse shown in Fig. 4(c). The dips represent an effect of depletion. As can be seen from the figure, this effect can be rather strong, especially at orientations near maxima of the ionization rate.

The dependence of the RWPs on the scattering angle θ is illustrated by the cuts shown in Fig. 5. The RWP gradually grows as θ decreases from $\theta = 180°$ corresponding to rescattering in the backward direction and attains a maximum near $\theta = 65°$. This behavior is determined by the variation of the kinematic characteristics of rescattering along the caustic.

To close this discussion of the RWP, we mention that in the original paper [8], where the idea of factorization was introduced, it was assumed that the RWP is a constant independent of the angle θ. However, an explicit analytical expression for the RWP derived in Ref. [13] contains an essential dependence on the angle, as illustrated in Figs. 3 and 5. The dependence on β is averaged out by the integration over β in Eq. (3b); to measure this dependence, the experiment should be performed with aligned molecules. However, the dependence on θ survives averaging. This dependence directly affects the shape of $S(\theta)$ obtained from Eq. (3b), and taking it into account was shown to considerably improve the agreement with theoretical [13] and experimental PEMDs [15, 16].

We now discuss the DCS factor in the integrand in Eq. (3b) obtained by averaging the DCS over the azimuthal scattering angle, Eq. (4). We have calculated this factor as a

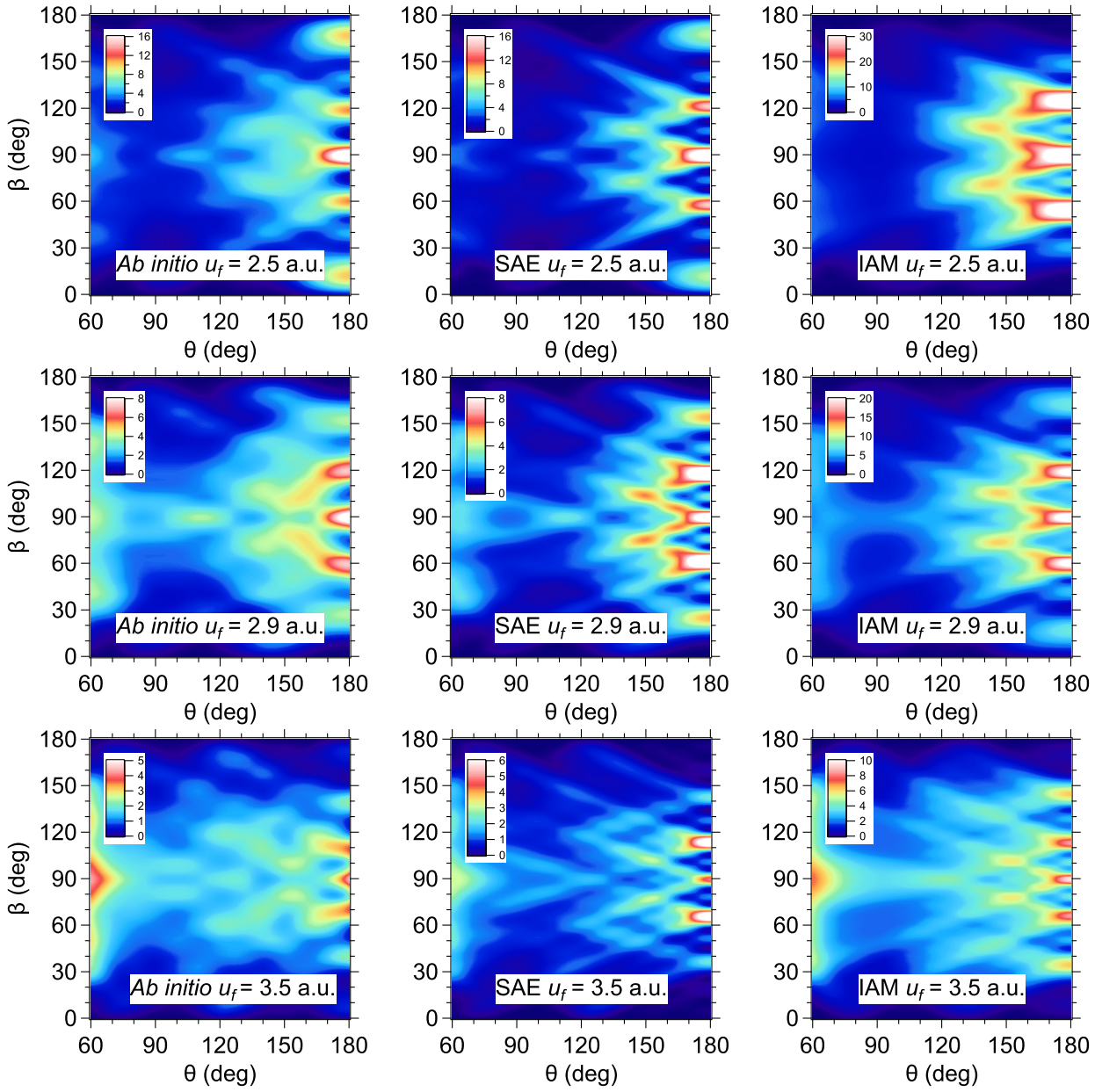

FIG. 6. Plots of the averaged DCS factor in Eq. (3b) multiplied by $\sin\beta$ as a function of the scattering angle θ and the alignment angle β calculated using *ab initio* (left column), SAE (middle column), and IAM (right column) methods. The values of u_f indicating the incident momentum coincide with incident momenta of backward ($\theta = 180°$) rescattering at the caustic for the 1300 nm (top row), 1450 nm (middle row), and 1650 nm (bottom row) laser pulses (see caption to Fig. 1).

function of the scattering angle θ and the alignment angle β for three values of the incident momentum u_f = 2.5 a.u., 2.9 a.u., and 3.5 a.u. coinciding with incident momenta of backward ($\theta = 180°$) rescattering at the caustic for the three pulses considered in the experiment (see caption to Fig. 1). For each u_f, the calculations were performed using *ab initio*, SAE, and IAM methods. The results obtained are shown in Fig. 6. The averaged DCSs demonstrate pronounced interference structures, especially at large scattering angles. All three methods used in scattering calculations reproduce qualitatively similar structures, although the details are different. The strong interference peaks at $\theta = 180°$ are produced by constructive interference of electrons scattered by the C and O centers. Indeed, consider, e.g., the peaks in the top middle panel located near $\beta = 90°$, 60° and 120°, etc. The condition of constructive C-O interference is $2u_f R\cos\beta = 0, \pm 2\pi$, etc., which gives $\beta = 90°$, 55° and 124°, etc. One can also notice weaker peaks located between the strong peaks. In the top middle panel they are seen near $\beta = 75°$ and 105°, etc. These peaks are produced by constructive interference of electrons scattered by the two O centers. Indeed, the condition of constructive O-O interference is $4u_f R\cos\beta = 0, \pm 2\pi$, etc., which gives $\beta = 90°$, 73° and 106°, etc. Thus, strong peaks contain contributions of both C-O and O-O interference, while weak peaks result from the O-O interference only. Note that the weak O-O interference peaks are not seen in the *ab initio* results; one can notice only two such peaks near $\beta = 40°$ and 140° in the top left panel. On the other hand, the SAE and IAM results reproduce O-O peaks at all values of u_f considered. All these peaks are direct fingerprints of the molecular geometry. At smaller θ, the strong peaks split into two peaks, producing a rich interference pattern in the interval $120° \leqslant \theta \leqslant 170°$. This pattern presents a more subtle image of the molecular structure. Its details essentially differ for the different methods of scattering calculations, and hence it is sensitive to the underlying structure model.

We have discussed the individual behavior of the two factors in the integrand in Eq. (3b) shown in Figs. 3 and 6. By performing the integration over β, we obtain results which can be compared with the experiment. The results obtained by the three scattering calculation methods are shown by lines in Fig. 2. From the comparison of the experimental and theoretical results *in general*, the following two conclusions can be drawn. First, although the averaged DCSs calculated by the different methods considerably differ from each other, see Fig. 6, the integration over β reduces the difference, so that the final results for $S(\theta)$ are rather similar. Second, the theoretical results are in fairly good agreement with the experi-

mental results for all three laser pulses considered. By inspecting Fig. 2 in more detail, one can notice some small-scale modulations in the experimental results. For example, there is a dip in the results for 1650 nm near $\theta = 150°$. This dip is reproduced by the *ab initio* and SAE calculations, but is absent in the IAM results. The origin of the dip can be traced back to a feature in the structure of the averaged DCSs. Consider, e.g., the *ab initio* results. For the 1650 nm pulse, the RWP at $\theta = 150°$ peaks near $\beta = 60°$ and 120°, see Fig. 3(c). At these values of θ and β, the averaged DCS shown in the bottom left panel of Fig. 6 has a local minimum. This minimum leads to the appearance of the dip in the *ab initio* results in Fig. 2(c) at $\theta = 150°$. One can notice similar local minima at $\theta = 150°$ and $\beta = 60°$ and 120° also in the bottom middle and right panels of Fig. 6. In the former case, this results in a more shallow dip in the SAE results in Fig. 2(c). However, in the latter case, a dip does not appear in the IAM results in Fig. 2(c), because the effect of the minima on the integral over β is compensated by two strong peaks in the averaged DCS located near $\beta = 80°$ and 100°. This analysis gives an example of how the fingerprints of the structure of the averaged DCSs can be uncovered in the experimental PEMDs.

One possible source of these minor difference between the IAM results and the SAE and *ab initio* results might be that the IAM calculation only uses scattering from neutral atoms and thus implicitly does not contain the effects of the long-range Coulomb potential that is found in both the SAE and *ab initio* calculations.

The first of the conclusions formulated above means that, unfortunately, the present experimental results do not enable us to unambiguously decide which of the three theoretical structure models used in scattering calculations works better. The results become insensitive to the model because of averaging over the molecular alignment angle β. To probe the difference between the structure of the averaged DCSs calculated by the different methods at a given β one should be able to limit experimental measurements to a narrow interval around this β. The RWP factor plays a role of a window function in Eq. (3b) which limits the interval of β effectively contributing to the integral. However, the present results show that such a localization in β is not sufficient. Moreover, it is passive, that is, the interval of β probed in the experiment is determined by molecular properties (by the shape of the RWP) and cannot be changed. Alternatively, an active localization in β is possible by performing measurements with aligned molecules, as it was done in Refs. [2, 3]. Note that a much narrower distribution in β can be obtained by aligning molecules in the direction of the

maximum of the RWP. The second of the conclusions and the discussion of modulations seen in Fig. 2 suggest that if experimental results are collected from a sufficiently narrow interval of β, the present theory should enable one to discriminate between different structure models.

V. CONCLUSION AND OUTLOOK

We presented an experimental and theoretical study on rescattering photoelectron spectroscopy of CO_2 molecules. Strong-field PEMDs generated by infrared laser pulses at 1300, 1450, and 1650 nm wavelengths were measured and analyzed on the basis of a recently developed adiabatic theory of rescattering [13]. The experimental PEMDs extracted along the outermost backward rescattering caustic are compared with theoretical results obtained from the analytical factorization formula derived in Ref. [13]. Several methods to calculate the target structure information needed to implement this formula are considered. It is shown that RWPs calculated within the SAE approximation and by the HF method have only minor differneces from each other. On the other hand, DCSs calculated by *ab initio*, SAE, and IAM methods are considerably different. The difference reveals itself in a rich interference structure of the DCSs as functions of the molecular alignment angle β and the photoelectron scattering angle θ. This structure is shown to reflect the molecular geometry encoded in the peaks at $\theta = 180^\circ$ produced by constructive interference of electrons scattered by the different atomic centers as well as to contain a more subtle target structure information encoded in the interference pattern in the interval $120^\circ \leqslant \theta \leqslant 170^\circ$. Unfortunately, the difference almost disappears after averaging theoretical results for a space-fixed molecule over random orientations of molecules in the present experiment. In general, theoretical results obtained by the different scattering calculation methods are in fairly good agreement with the experimental results. Moreover, the *ab initio* and SAE calculations reproduce some small modulations seen in the experimental results, and we showed how the origin of these modulations can be related to the behavior of the DCS. However, because of the averaging over molecular orientations, the present experimental results do not enable us to resolve details in the behavior of the DCSs and discriminate between the different target structure models underlying the scattering calculations. Similar experimental measurements with aligned molecules are needed to judge which model describes the DCS more accurately.

This is a direction for future studies. We mention that it would also be extremely interesting to perform such measurements for linear molecules with the HOMO of π symmetry, like the CO_2 molecule, aligned along the polarization axis, to extend rescattering photoelectron spectroscopy to vortex electrons [36].

ACKNOWLEDGMENTS

This work was supported in part by grants-in-aid for scientific research from Japan Society for the Promotion of Science (JSPS), by the X-ray Free Electron Laser Utilization Research Project and the X-ray Free Electron Laser Priority Strategy Program of the Ministry of Education, Culture, Sports, Science and Technology of Japan, Dynamic Alliance for Open Innovation Bridging Human, Environment and Materials, IMRAM research program, and JSPS KAKENHI Grand No. 17K05739. A. I. D. and O. I. T. acknowledge support from the Ministry of Education and Science of Russia (State Assignment No. 3.873.2017/4.6) and the Russian Foundation for Basic Research (Grant No. 17-02-00198). T. M. was supported in part by JSPS KAKENHI Grants No. 17K05597 and No. 19H00887. Work performed at LBNL was supported by the U.S. Department of Energy, Office of Science, Basic Energy Sciences, Chemical Sciences, Geosciences, and Biosciences Division under contract number DE-AC02-05CH11231.

[1] C. I. Blaga, J. Xu, A. D. DiChiara, E. Sistrunk, K. Zhang, P. Agostini, T. A. Miller, L. F. DiMauro, and C. D. Lin, "Imaging ultrafast molecular dynamics with laser-induced electron diffraction," Nature **483**, 194–197 (2012).

[2] M. G. Pullen, B. Wolter, A.-T. Le, M. Baudisch, M. Hemmer, A. Senftleben, C. D. Schröter, J Ullrich, R. Moshammer, C. D. Lin, and J. Biegert, "Imaging an aligned polyatomic molecule with laser-induced electron diffraction," Nat. Comm. **6**, 7262 (2015).

[3] B. Wolter, M. G. Pullen, A.-T. Le, M. Baudisch, K. Doblhoff-Dier, A. Senftleben, M. Hemmer, C. D. Schroeter, J. Ullrich, T. Pfeifer, R. Moshammer, S. Graefe, O. Vendrell, C. D. Lin, and J. Biegert, "Ultrafast electron diffraction imaging of bond breaking in di-ionized acetylene," Science **354**, 308–312 (2016).

[4] Y. Ito, C. Wang, A.-T. Le, M. Okunishi, D. Ding, C. D. Lin, and K. Ueda, "Extracting conformational structure information of benzene molecules via laser-induced electron diffraction," Structural Dynamics **3**, 034303 (2016).

[5] Y. Ito, R. Carranza, M. Okunishi, R. R. Lucchese, and K. Ueda, "Extraction of geometrical structure of ethylene molecules by laser-induced electron diffraction combined with ab initio scattering calculations," Phys. Rev. A **96**, 053414 (2017).

[6] T. Zuo, A. D. Bandrauk, and P. B. Corkum, "Laser-induced electron diffraction: a new tool for probing ultrafast molecular dynamics," Chem. Phys. Lett. **259**, 313 – 320 (1996).

[7] M. Meckel, D. Comtois, D. Zeidler, A. Staudte, D. Pavičić, H. C. Bandulet, H. Pépin, J. C. Kieffer, R. Dörner, D. M. Villeneuve, and P. B. Corkum, "Laser-induced electron tunneling and diffraction," Science **320**, 1478–1482 (2008).

[8] T. Morishita, A.-T. Le, Z. Chen, and C. D. Lin, "Accurate retrieval of structural information from laser-induced photoelectron and high-order harmonic spectra by few-cycle laser pulses," Phys. Rev. Lett. **100**, 013903 (2008).

[9] M. Okunishi, T. Morishita, G. Prümper, K. Shimada, C. D. Lin, S. Watanabe, and K. Ueda, "Experimental retrieval of target structure information from laser-induced rescattered photoelectron momentum distributions," Phys. Rev. Lett. **100**, 143001 (2008).

[10] D. Ray, B. Ulrich, I. Bocharova, C. Maharjan, P. Ranitovic, B. Gramkow, M. Magrakvelidze, S. De, I. V. Litvinyuk, A.-T. Le, T. Morishita, C. D. Lin, G. G. Paulus, and C. L. Cocke, "Large-angle electron diffraction structure in laser-induced rescattering from rare gases," Phys. Rev. Lett. **100**, 143002 (2008).

[11] M. Okunishi, H. Niikura, R. R. Lucchese, T. Morishita, and K. Ueda, "Extracting electron-ion differential scattering cross sections for partially aligned molecules by laser-induced rescattering photoelectron spectroscopy," Phys. Rev. Lett. **106**, 063001 (2011).

[12] C. Wang, M. Okunishi, R. R. Lucchese, T. Morishita, O. I. Tolstikhin, L. B. Madsen, K. Shimada, D. Ding, and K. Ueda, "Extraction of electron-ion differential scattering cross sections for C_2H_4 by laser-induced rescattering photoelectron spectroscopy," J. Phys. B **45**, 131001 (2012).

[13] T. Morishita and O. I. Tolstikhin, "Adiabatic theory of strong-field photoelectron momentum distributions near a backward rescattering caustic," Phys. Rev. A **96**, 053416 (2017).

[14] O. I. Tolstikhin and T. Morishita, "Adiabatic theory of ionization by intense laser pulses: Finite-range potentials," Phys. Rev. A **86**, 043417 (2012).

[15] H. Geiseler, N. Ishii, K. Kaneshima, F. Geier, T. Kanai, O. I. Tolstikhin, T. Morishita, and J. Itatani, "Carrier-envelope phase mapping in laser-induced electron diffraction," Phys. Rev. A **94**, 033417 (2016).

[16] Y. Ito, M. Okunishi, T. Morishita, O. I. Tolstikhin, and K. Ueda, "Rescattering photoelectron spectroscopy of heterodiatomic molecules with an analytical returning photoelectron wave packet," Phys. Rev. A **97**, 053411 (2018).

[17] A. R. Edmonds, *Angular Momentum in Quantum Mechanics* (Princeton University Press, Princeton, 1957).

[18] G. G. Paulus, W. Becker, W. Nicklich, and H. Walther, "Rescattering effects in above-threshold ionization: a classical model," J. Phys. B **27**, L703 (1994).

[19] P. A. Batishchev, O. I. Tolstikhin, and T. Morishita, "Atomic Siegert states in an electric field: Transverse momentum distribution of the ionized electrons," Phys. Rev. A **82**, 023416 (2010).

[20] L. Hamonou, T. Morishita, and O. I. Tolstikhin, "Molecular Siegert states in an electric field," Phys. Rev. A **86**, 013412 (2012).

[21] V. N. T. Pham, O. I. Tolstikhin, and T. Morishita, "Molecular Siegert states in an electric field. II. Transverse momentum distribution of the ionized electrons," Phys. Rev. A **89**, 033426 (2014).

[22] O. I. Tolstikhin, T. Morishita, and L. B. Madsen, "Theory of tunneling ionization of molecules: Weak-field asymptotics including dipole effects," Phys. Rev. A **84**, 053423 (2011).

[23] L. B. Madsen, O. I. Tolstikhin, and T. Morishita, "Application of the weak-field asymptotic theory to the analysis of tunneling ionization of linear molecules," Phys. Rev. A **85**, 053404 (2012).

[24] A. I. Dnestryan and O. I. Tolstikhin, "Integral-equation approach to the weak-field asymptotic theory of tunneling ionization," Phys. Rev. A **93**, 033412 (2016).

[25] A. I. Dnestryan, O. I. Tolstikhin, L. B. Madsen, and F. Jensen, "Structure factors for tunneling ionization rates of molecules: General grid-based methodology and convergence studies," J. Chem. Phys. **149**, 164107 (2018).

[26] M. W. Schmidt, K. K. Baldridge, J. A. Boatz, S. T. Elbert, M. S. Gordon, J. H. Jensen, S. Koseki, N. Matsunaga, K. A. Nguyen, S. Su, T. L. Windus, M. Dupuis, and J. A. Montgomery Jr, "General Atomic and Molecular Electronic Structure System," J. Comput. Chem. **14**, 1347 (1993).

[27] R. H. Garvey, C. H. Jackman, and A. E. S. Green, "Independent-particle-model potentials for atoms and ions with $36 < Z \leq 54$ and a modified Thomas-Fermi atomic energy formula," Phys. Rev. A **12**, 1144 (1975).

[28] L. Wang, J. E. Reutt, Y. T. Lee, and D. A. Shirley, "High resolution UV photoelectron spectroscopy of CO_2, COS, and CS_2 using supersonic molecular beams," J. Electron Spectrosc. Relat. Phenom. **47**, 167 (1988).

[29] V. P. Majety and A. Scrinzi, "Static field ionization rates for multi-electron atoms and small molecules," J. Phys. B **48**, 245603 (2015).

[30] "NIST electron elastic-scattering cross-section database: Version 3.2," NIST Standard Reference Database Number 64.

[31] F. Salvat, A. Jablonski, and C. J. Powell, "ELSEPA — Dirac partial-wave calculation of elastic scattering of electrons and positrons by atoms, positive ions and molecules," Comput. Phys. Commun. **165**, 157–190 (2005).

[32] F. A. Gianturco, R. R. Lucchese, and N. Sanna, "Calculation of low-energy elastic cross sections for electron-CF_4 scattering," J. Chem. Phys. **100**, 6464–6471 (1994).

[33] Alexandra P. P. Natalense and Robert R. Lucchese, "Cross section and asymmetry parameter calculation for sulfur 1s photoionization of SF_6," J. Chem. Phys. **111**, 5344–5348 (1999).

[34] Jr. Dunning, Thom H., "Gaussian basis sets for use in correlated molecular calculations. I. the atoms boron through neon and hydrogen," J. Chem. Phys. **90**, 1007–1023 (1989).

[35] Rick A. Kendall, Jr. Dunning, Thom H., and Robert J. Harrison, "Electron affinities of the first-row atoms revisited. Systematic basis sets and wave functions," J. Chem. Phys. **96**, 6796–6806 (1992).

[36] O. I. Tolstikhin and T. Morishita, "Strong-field ionization, rescattering, and target structure imaging with vortex electrons," Phys. Rev. A **99**, 063415 (2019).